CHEMICAL ENGINEERING TRANSACTIONS
VOL. 103, 2023
A publication of AIDIC
The Italian Association of Chemical Engineering
Online at www.cetjournal.it
Guest Editors: Petar S. Varbanov, Panos Seferlis, Yee Van Fan, Athanasios Papadopoulos

ISBN 979-12-81206-02-1; **ISSN** 2283-9216
DOI: 10.3303/CET23103012

Numerical Investigation of Methane Steam Reforming in the Packed Bed Installed with Metal Foam

Zhihong Wu, Jian Yang, Qiuwang Wang*

Key Laboratory of Thermo-Fluid Science and Engineering, MOE, School of Energy and Power Engineering, Xi'an Jiaotong University, Xi'an, Shaanxi, 710049, P.R. China
wangqw@mail.xjtu.edu.cn

Hydrogen is one of the vital energy sources for addressing climate change, and methane steam reforming via a packed bed reactor is a primary method for global hydrogen supply. Recently, to enhance heat transfer, metal foam become the focus of research, and the heat transfer performance of reactors significantly affects hydrogen production. Therefore, it is one of the promising approaches to install the metal foam inside the packed bed reactor for higher hydrogen production. In this study, the methane steam reforming in the packed bed reactors installed with the different metal foams has been investigated by numerical method. It was found that the installation of metal foam leads to the increment of average velocity and the decrease of pressure drop, which is increased by 7.69 % and decreased by 4.82 % at maximum. Besides, the heat transfer performance was improved after the installation of metal foam, the temperature increased by 68.07 K at maximum and the overall heat transfer coefficient increased by 10.64 %. Due to the better performance of flow and heat transfer, the overall efficiency of hydrogen production is increased by 23.21 %.

1. Introduction

Excess carbon emission introduces global warming and other environmental challenges as a result of the use of fossil fuels (Oner and Dincer, 2023). Hydrogen become one of the promising alternatives to fossil fuel and can effectively settle environmental challenges, which has the advantages of high calorific value, low emissions, and multipurpose raw material. There are many studies about the methods of hydrogen production, such as, via dark fermentation of bacteria (Vadalà et al., 2023), through operating Rankine cycle-based fuel cell (Sathish et al., 2023), and from plastic waste pyrolysis (Al-Fatesh et al., 2023). Yet, the traditional method has still been the main may for hydrogen production. Methane steam reforming accounts for 60 % of global hydrogen production (IEA, 2021), which will be the primary method in the next 20 y.
Wu et al. (2020) studied the reactor of different catalyst particle distributions with variable diameters in the axial direction and pointed out that this distribution contributes to higher efficiency. Mokheimer et al. (2014) studied the effects of different operating parameters on methane steam reforming via the equivalent medium method. Lao et al. (2016) compared the numerical results of the equivalent medium method with the industry data and pointed out the accuracy of this method. The equivalent medium method has been used in this study. In the process of methane steam reforming, the packed bed reactor is the key equipment. Yuan et al. (2017) found out that there is a lower temperature zone near the inlet of the reactor, which limits the efficiency of the reactor. To enhance heat transfer performance, it is a promising method for installing metal foam in the packed bed reactor. In this study, the methane steam reforming in the packed bed installed with metal foam has been investigated. The reactors with different metal foams were compared from flow, heat transfer, and reaction. The enhancement has been evaluated and the mechanism was analysed.

2. Methods

The methods of this study have been illustrated in this section in five parts: physical model, governing equations, reaction mechanism, boundary conditions and method validation. The details are shown as follows.

Paper Received: 15 March 2023; Revised: 12 April 2023; Accepted: 08 June 2023
Please cite this article as: Wu Z., Yang J., Wang Q., 2023, Numerical Investigation of Methane Steam Reforming in the Packed Bed Installed with Metal Foam, Chemical Engineering Transactions, 103, 67-72 DOI:10.3303/CET23103012

2.1 Physical model

The multi-tubular packed bed reactor is commonly used in industry. In this study, a single tube installed with catalyst particles and metal foam has been used to investigate. The tube is divided into two zones, the zone of packed catalyst and the zone of metal foam. As detectable in Figure 1, the physical model and the geometry parameters are shown. The catalyst particles are sphere-type with a 12 mm diameter.

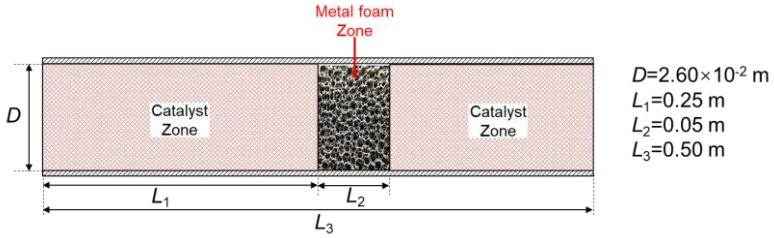

Figure 1: The diagram of a single tube installed with catalyst and metal foam and the geometry parameters

2.2 Governing equations

The equivalent medium method was used to study the methane steam reforming, in which the catalyst zone was treated as a porous medium with reactions proceeding. In the metal foam zone, the Darcy extended Forchheimer flow model and local thermal non-equilibrium model were adopted in the simulation. Besides, there are no reactions proceeding in this zone. The main governing equations are presented in Table 1. As shown in Table 1, u_i, x_i, ρ_f, p, μ, I, T, λ_{eff}, C_p, h_m, J_{mj}, $\lambda_{f,eff}$, h_{sf}, a_{sf}, T_s, T_f, $\lambda_{s,eff}$, Y_m, R_m represents the velocity in the direction i, the cartesian coordinates in the direction i, the density of the fluid, the pressure, the dynamic viscosity, the unit tensor, temperature, the effective thermal conductivity, the specific heat capacity, the formation standard enthalpy of species m, the diffusion flux of species m in direction j, the effective thermal conductivity of fluid, the interfacial heat transfer coefficient, the interfacial surface area, the solid temperature, the fluid temperature, the effective thermal conductivity of solid, the mass fraction of species m and the generation or consumption rate of species m. S_i and S_h are the momentum source term and the energy source term. All equations involved are coupled by using finite volume analysis software ANSYS Fluent software, in which the SIMPLE algorithm is employed and the reaction rate was calculated by the User Defined Functions.

Table 1: The main governing equations in the simulation

	Catalyst zone	*Metal foam zone*
Continuity	$\frac{\partial u_i}{\partial x_i} = 0$	$\frac{\partial u_i}{\partial x_i} = 0$
Momentum	$\frac{\partial \rho_f u_i u_j}{\partial x_j} = -\frac{\partial p}{\partial x_j} + \frac{\partial}{\partial x_j}\left[\mu\left(\frac{\partial u_i}{\partial x_j} + \frac{\partial u_j}{\partial x_i}\right) - \frac{2}{3}\frac{\partial u_i}{\partial x_j} I\right] + S_{i,1}$	$\frac{\partial \rho_f u_i u_j}{\partial x_j} = -\frac{\partial p}{\partial x_j} + \frac{\partial}{\partial x_j}\left[\mu\left(\frac{\partial u_i}{\partial x_j} + \frac{\partial u_j}{\partial x_i}\right) - \frac{2}{3}\frac{\partial u_i}{\partial x_j} I\right] + S_{i,2}$
Energy	$\frac{\partial \rho_f u_i T}{\partial x_i} = \frac{\partial}{\partial x_j}\left(\frac{\lambda_{eff}}{C_p}\frac{\partial T}{\partial x_j}\right) - \frac{\partial}{\partial x_j}\left(\sum_m h_m J_{mj}\right) + S_h$	Fluid phase: $\frac{\partial\left(\rho_f C_p u_i T\right)}{\partial x_i} = \frac{\partial}{\partial x_i}\left(\lambda_{f,eff}\frac{\partial T}{\partial x_i}\right) + h_{sf} a_{sf}\left(T_s - T_f\right)$ Solid phase: $0 = \frac{\partial}{\partial x_i}\left(\lambda_{s,eff}\frac{\partial T}{\partial x_i}\right) - h_{sf} a_{sf}\left(T_s - T_f\right)$
Species	$\frac{\partial}{\partial x_j}\left(\rho_f u_j Y_m\right) = -\frac{\partial}{\partial x_j}\left(J_{mj}\right) + R_m$	

2.3 Reaction mechanism

The kinetic model of Xu and Froment (1989) was used. There are three main reactions considered in the simulation, and the reaction rates are also shown below.

Reaction 1: $CH_4 + H_2O \rightleftarrows CO + 3H_2$, $\Delta H^0_{298} = 206\ \mathrm{kJ/mol}$ (1)

Reaction 2: $\mathrm{CO}+\mathrm{H_2}O \rightleftarrows \mathrm{CO_2}+\mathrm{H_2}$, $\Delta H_{298}^{0} = -41.1\ \mathrm{kJ/mol}$ (2)

Reaction 3: $\mathrm{CH_4}+2\mathrm{H_2}O \rightleftarrows \mathrm{CO_2}+4\mathrm{H_2}$, $\Delta H_{298}^{0} = 164.9\ \mathrm{kJ/mol}$ (3)

$$r_1 = \frac{k_1\left(p_{\mathrm{CH_4}}p_{H_2O} - \frac{p_{H_2}^3 p_{\mathrm{CO}}}{K_1}\right)}{p_{H_2}^{2.5}(\mathrm{DEN})^2} \quad (4)$$

$$r_2 = \frac{k_2\left(p_{\mathrm{CO}}p_{H_2O} - \frac{p_{H_2}p_{\mathrm{CO_2}}}{K_2}\right)}{p_{H_2}(\mathrm{DEN})^2} \quad (5)$$

$$r_3 = \frac{k_3\left(p_{\mathrm{CH_4}}p_{H_2O}^2 - \frac{p_{H_2}^4 p_{\mathrm{CO_2}}}{K_3}\right)}{p_{H_2}^{3.5}(\mathrm{DEN})^2} \quad (6)$$

$$\mathrm{DEN}=1+K_{\mathrm{CO}}p_{\mathrm{CO}} + K_{H_2}p_{H_2} + K_{\mathrm{CH_4}}p_{\mathrm{CH_4}} + K_{H_2O}p_{H_2O}/p_{H_2} \quad (7)$$

where r_1, r_2 and r_3 represent the reaction rates of three reactions: Reaction 1, Reaction 2 and Reaction 3. k_1, k_2 and k_3 represent the rate coefficients of three reactions. K_1, K_2 and K_3 are the equilibrium constants of the three reactions. K_{CO}, K_{H_2}, K_{H_2O} and K_{CH_4} represent the adsorption constants of three species, p_{CH_4}, p_{H_2}, p_{CO}, p_{CO_2} and p_{H_2O} are the partial pressures of different species.

2.4 Boundary conditions

The SST-kω turbulence flow model was adopted in this study, and the *Re* is about 8500. The boundary conditions and the properties of the catalyst and the metal foams (Jadhav et al., 2021) were presented in Tables 2-3. As observable in Table 2, V_{in}, T_{in}, q_{wall}, ϕ_{CH4}, ϕ_{H2O}, ρ_c,$C_{p,c}$, K_c represents the inlet velocity, the inlet temperature, the wall heat flux, the methane mass fraction at the inlet, the water vapour mass fraction at inlet, the density of catalyst, the specific heat of catalyst and the thermal conductivity of the catalyst. In Table 3, PPI, D_f, D_p, ε, K, C represent the pores per linear inch, the fibre diameter, the pore diameter, the porosity, permeability and form drag coefficient.

Table 2: Boundary conditions for simulation and properties of the catalyst

V_{in} (m/s)	T_{in} (K)	q_{wall} (W/m^2)	ϕ_{CH4} (-)	ϕ_{H2O} (-)	ρ_c (kg·m^{-3})	$C_{p,c}$ (J·kg^{-1}·K^{-1})	K_c (W·m^{-1}·K^{-1})
4.00	773.15	30,000.00	0.20	0.80	1,947.00	1,000.00	1.00

Table 3: Properties of different metal foam (Jadhav et al. 2021)

Name	*Material*	*PPI*	D_f (10^{-4} m)	D_p (10^{-3} m)	ε	a_{sf} (m^{-1})	h_{sf} (W·m^{-2}·K^{-1})	K (10^{-7} m^2)	C (m^{-1})
MF-1		10	4.45	4.95	0.95	360.60	2,209.34	2.48	94.98
MF-2	Stainless	20	4.51	3.42	0.90	960.65	1,987.88	2.18	208.82
MF-3	steel-316	30	2.16	2.32	0.92	936.38	2,927.22	1.64	148.97
MF-4		40	1.84	1.65	0.90	1,671.76	3,112.21	4.20	397.01

2.5 Method validation

The model validation was compared with the work of Mokheimer et al. (2014). In the validation, the operating pressure was set as 1,000,000 Pa, and the T_{in} was set as 848 K, 838 K and 798 K, 773 K, which was same as T_{in}. The results of the methane conversion rate are shown in Figure 2a. The maximum deviations are 10.92 %, 9.20 %,12.60 % and 7.25 % for three temperature cases. The average deviations range from 2.36 % to 6.23 %. The mesh independence has been validated, as shown in Figure 2b. The quantities of mesh range from 1,428 to 39,904, and the methane conversion rate was focused on. As the mesh quantity is larger than 20,667, the deviations are no more than 0.1 %. At last, the global size of the mesh was set as 0.7 mm, and the height of the first boundary layer was set as 0.1 mm.

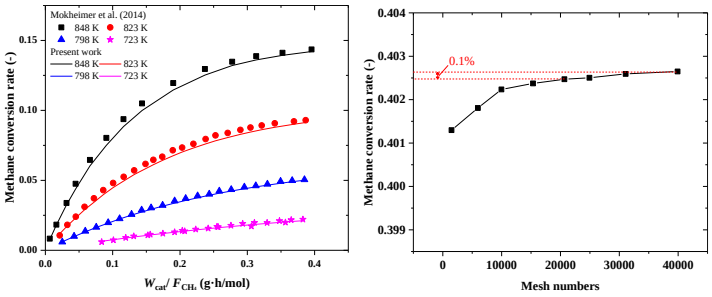

(a) (b)

Figure 2: The validation of (a) method compared with Mokheimer et al. (2014) and (b) mesh independence

3. Results and discussions

Different reactors were compared in the same condition. To evaluate the performance of reactors, the results have been investigated from the heat transfer, flow and reaction mechanism.

3.1 Flow performance

The comparison of velocity contours among different reactors has been shown in Figure 3. Because of the higher porosity, the installation of metal foam increases the average velocity (*V*) as detectable in Figure 3.

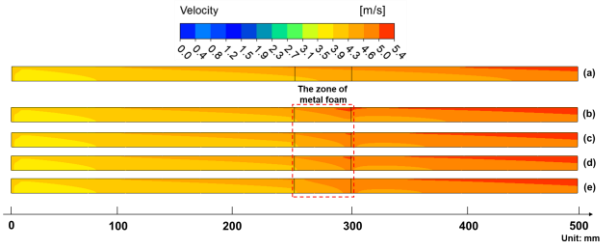

Figure 3: Velocity contours of different reactors: (a) N, (b) MF-1, (c) MF-2, (d) MF-3 and (e) MF-4

Figure 4a depicts the *V* distribution in the axial direction, in which the *V* increases after the zone of metal foam ($0.5 < A/L < 0.6$, where the A/L represents the ratio of the axial distance to the reactor length). The *V* is increased by 7.69 % at maximum compared with the N (The N represents the normally packed bed reactor with no metal porous). As observable in Figure 4b, compared with the N, the MF-1, MF-2, and MF-3 have lower pressure drop per unit length ($\Delta p/L$). However, the MF-4 leads to the increment of $\Delta p/L$. The $\Delta p/L$ of MF-1 is decreased by 4.82 % and the $\Delta p/L$ of MF-4 is increased by 10.18 %. The MF-1, MF-2 and MF-3 have better flow performance.

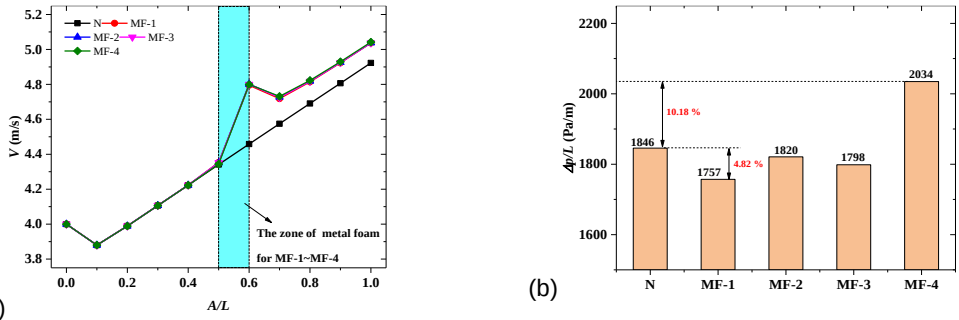

(a) (b)

Figure 4: Comparison of (a) velocity (V) distribution in the axial direction and (b) pressure drop per unit length ($\Delta p/L$)

3.2 Heat transfer performance

As shown in Figure 5, the temperature contours of different reactors have been compared. Obviously, because there is no reaction proceeding and velocity is higher in the zone of metal foam, more heat transfers in the radial direction, which leads to the higher average temperature in this zone. With comparing the MF-1 and the MF-4, the temperature of MF-1 in the zone near the wall is higher than the MF-4. The reason is that the velocity is

higher in the zone near the wall of MF-1 according to the Figures 3b and 3e, the convective heat transfer is enhanced.

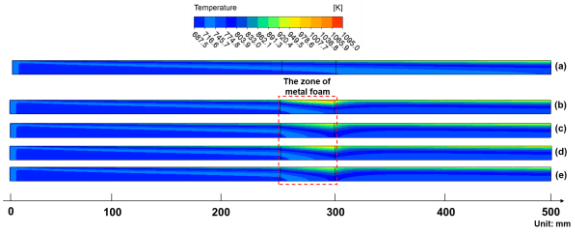

Figure 5: Temperature contours of different reactors: (a) N, (b) MF-1, (c) MF-2, (d) MF-3 and (e) MF-4

Figure 6a depicts the temperature (*T*) distribution in the axial direction, in which the installation of metal foam leads to the increment of *T*. The *T* is increased by 68.07 K compared with the N. As for the comparison of overall heat transfer coefficient (γ), the MF-1, MF-2 and MF-3 have a higher value than the N as observable in Figure 6b. The γ of MF-1 is increased by 10.64 %. The results are consistence with the reference (Jadhav et al., 2021), in which metal foam contributes to better performance of heat transfer.

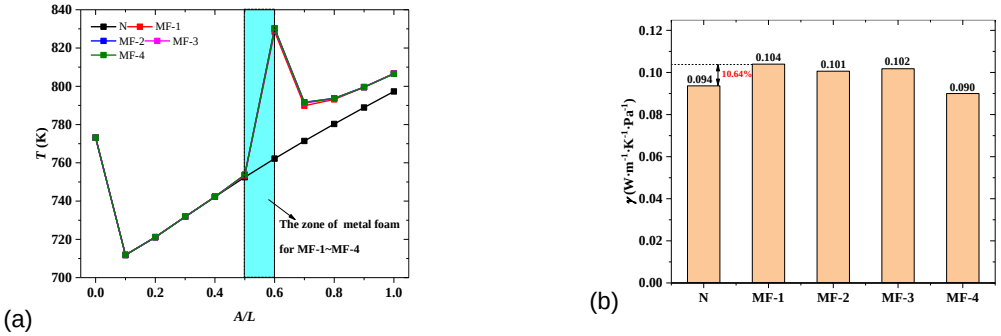

Figure 6: Comparison of (a) temperature (T) distribution in the axial direction and (b)overall heat transfer coefficient (γ)

3.3 Hydrogen production comparison

The hydrogen mass fraction of different reactors has been compared firstly. As observable in Figure 7a, the installation of metal foam leads to a higher hydrogen mass fraction after the zone of metal foam. The reaction rate of hydrogen production (R_{H2}) has been compared in Figure 7a. The R_{H2} equals zero in the zone of metal foam. Because the reaction rate depends on the temperature, there is higher R_{H2} after the zone of metal foam due to the enhancement of heat transfer. The R_{H2} of MF-1 is about 10 times higher than that of N.

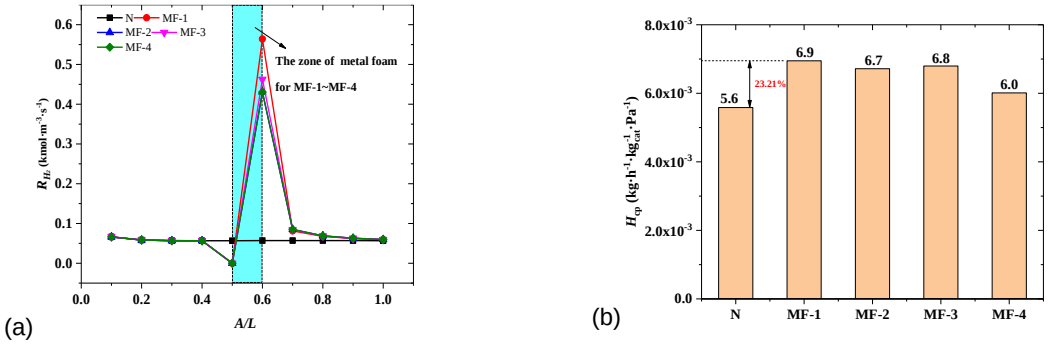

Figure 7: Comparison of (a) reaction rate of hydrogen production (RH2) and (b) hydrogen mass flow per catalyst mass per pressure drop

To evaluate the overall efficiency of hydrogen production, the hydrogen mass flow per catalyst mass per pressure drop (H_{cp}) has been used. It is obvious that the installation of metal foam leads to the increase in overall efficiency as shown in Figure 7b. The MF-1 has the highest H_{cp}, which is increased by 23.21 % compared

with the N. The results illustrate that there is less catalyst and lower flow losses for higher hydrogen production because of the installation of metal foam.

4. Conclusions

In this study, the methane steam reforming in different packed bed reactors installed with metal foam was numerically studied. The investigation compared heat transfer, flow and hydrogen production. A comparison of the overall heat transfer coefficient among different reactors was conducted. Considering the amount of usage catalyst and flow loss, the hydrogen mass flow per catalyst mass per pressure drop was used to evaluate the overall efficiency of hydrogen production. The results can guide hydrogen production for higher efficiency and less cost. The main findings are shown below.

1) As for flow performance, the installation of metal foam can improve the flow performance of the packed bed reactor. Because of higher porosity, the average velocity increases in the reactors, which is increased by 7.69 % at maximum. While the metal foam with suitable geometry parameters is used, the pressure drop will decrease, which is reduced by 4.82 % at maximum.

2) As regards heat transfer, because there are no reactions proceeding and velocity is higher, more heat transfers from the wall into the fluid through the metal foam. The temperature is increased by 68.07 K at maximum, and the overall heat transfer coefficient is increased by 10.64 %. The installation of metal foam leads to the better heat transfer performance of packed bed reactors.

3) Considering the amount of usage catalyst and flow losses, the hydrogen mass flow per catalyst mass per pressure drop was adopted to evaluate the overall efficiency of hydrogen production. The better performance of flow and heat transfer leads to higher overall efficiency in the reactors installed with metal foams, which is increased by 23.21 % at maximum.

Acknowledgments

This work was financially supported by the National Natural Science Foundation of China (Grant No. 52130609) and the Foundation for Innovative Research Groups of the National Natural Science Foundation of China (No. 51721004).

References

Al-Fatesh A.S., AL-Garadi N.Y.A., Osman A.I., Al-Mubaddel F.S., Ibrahim A.A., Khan W.U., Alanazi Y.M., Alrashed M.M., Alothman O.Y., 2023, From plastic waste pyrolysis to Fuel: Impact of process parameters and material selection on hydrogen production. Fuel, 344, 128107.

International Energy Agency, 2021, Global Hydrogen Review, 108, France. <iea.blob.core.windows.net/assets/5bd46d7b-906a-4429-abda-e9c507a62341/GlobalHydrogenReview2021.pdf>, accessed October 2021.

Jadhav P.H., Gnanasekaran N., Perumal D.A., Mobedi M., 2021, Performance evaluation of partially filled high porosity metal foam configurations in a pipe. Applied Thermal Engineering, 194,117081.

Lao L., Aguirre A., Tran A., Wu Z., Durand H., Christofides P.D., 2016, CFD modeling and control of a steam methane reforming reactor. Chemical Engineering Science, 148, 78-92.

Mokheimer E.M.A., Ibrar Hussain M., Ahmed S., Habib M.A., Al-Qutub A.A., 2014, On the modeling of steam methane reforming. Journal of Energy Resources Technology, 137, 012001.

Oner O., Dincer I., 2023, Numerical investigation of hydrogen production from low-pressure microwave steam plasma. Computers & Chemical Engineering, 174, 108230.

Sathish T., Sailaja C., Saravanan R., Suresh P., Anish M., Rajasimman M., Sambath U., Sabarirajan N., Muthukumar K., Joo S., Vasseghian Y., Raissi K., 2023, An absorber of parabolic trough collector for hydrogen production in a solid oxide fuel cell. Fuel, 343, 127982.

Vadalà M., Kröll E., Küppers M., Lupascu D.C., Brunstermann R., 2023, Hydrogen production via dark fermentation by bacteria colonies on porous PDMS-scaffolds, International Journal of Hydrogen Energy, DOI: 10.1016/j.ijhydene.2023.03.285.

Wu Z., Wang J., Yang J., Wang Q., 2020, Numerical Simulation on Methane Steam Reforming in Grille-sphere Composite Packed Bed with Axial Variable Diameter Configuration Particle. Chemical Engineering Transactions, 81, 1177-1182.

Xu J., Froment G.F., 1989, Methane Steam Reforming, Methanation and Water–Gas Shift: I. Intrinsic Kinetics. AIChE J, 35, 88–96.

Yuan Q., Gu R., Ding J., Lu J., 2017, Heat transfer and energy storage performance of steam methane reforming in a tubular reactor. Applied Thermal Engineering, 125, 633-643.